

Low frequency interactions between coupled narrow sidebranch arrays and the resulted sound transmission losses

H.M.Yu and S.K.Tang*

Department of Building Services Engineering
The Hong Kong Polytechnic University
Hong Kong
China

*Corresponding author. Tel.: +852 27667782; fax: +852 27657198
Email address : shiu-keung.tang@polyu.edu.hk (S.K. Tang)

Abstract

The low frequency sound interactions between coupled narrow sidebranch arrays installed in an infinitely long rectangular duct are investigated numerically using the finite-element method in the present study. The corresponding transmission losses achieved these coupled sidebranch arrays are also examined. The interactions between the coupled sidebranch arrays result in both dipole-like and quadrupole-like radiations into the main duct. Results show that the coupling of two sidebranch arrays of different sidebranch length series side-by-side on one side of the duct wall can improve the performance in term of spectral uniformity of sound transmission loss compared with the cases where only one array covers the whole spanwise width of the duct. The installation of two coupled arrays on opposite sides of the duct cross-section improves the magnitudes of the sound transmission loss in general. The performance of the coupled array system can be further enhanced by removing the separating wall between sub-arrays of one of the coupled sidebranch arrays. It is also found that reversing the sidebranch arrangement of one of the coupled arrays is detrimental to the low frequency performance of the array system.

Keywords

Low frequency duct noise; silencing device; sound transmission loss

1. Introduction

The traditional method to attenuate the air conditioning and ventilation system noise is by installing dissipative silencers into the ductwork [1]. These silencers in general consist of a constricted air passage with porous internal surfaces. The constrictions and the porous surfaces result in relatively high pressure head loss across the silencers such that more powerful (and thus noisier) fans are required to deliver the required air flow rate. This in turn increases the loading of the noise attenuation system, leading to excessive waste of electrical energy. However, porous materials are not effective noise absorbers at low frequencies [1]. They are also not useful in ducts conveying greasy/dirty/humid air and cannot be used in areas where stringent hygiene control is necessary.

Huang and Choy [2] introduced the drum-like silencer recently. However, the maintenance of the membrane tension is practically not easy and there is also a risk of turbulence-induced sound radiation [3]. Again, the dirty precipitation from the air moving along the ductwork will also downgrade the performance of such silencer design. The situations of silencing devices installed with micro-perforated membranes/panels/tubes, such as that of Allam and Åbom [4], are facing similar problems. Active noise control technique [5] can produce significant noise attenuation at low frequencies, but the accuracy of the required signal pickup will be largely reduced by the hostile environments inside practical ductwork.

Passive reactive silencers are also commonly used for attenuating air conditioning and ventilation system noise because of their stable performance. The absence of porous materials makes them suitable for use in hospitals and in dirty environment. Typical examples of such silencers include the plenum/expansion chambers [6], Helmholtz resonators [7], Herschel–Quincke tubes [8], quarter wavelength tubes [9] and there are also many derivatives proposed in the past few decades. These silencers are resonance-based devices and thus their working frequency bandwidths are usually narrow. While it is possible to widen the working bandwidth by coupling reactive devices, such as those in Seo and Kim [10] and Howard et al. [11], a careful selection of resonance

frequencies is required. The resulting device can also be bulky. Tang [12] illustrated the broadband sound transmission losses (TL) across a duct section with relatively compact narrow sidebranch arrays installed flushed with the duct walls. The overall longitudinal lengths of the arrays are about 10% longer than the duct width. The sidebranch interactions responsible for the high sound transmission losses were also explained by Tang [12].

The sound transmission loss spectrum of a single wall mounted sidebranch array is spurious and consists of TL troughs at less than or equal to 5 dB between the TL peaks. To remedy such deficiency, Tang [12] introduced an additional array of the same longitudinal length but with sidebranches of a different length series on the opposite side of the duct. The overall silencer then becomes a bit bulky. In this study, the possibility of improving array acoustical performances by introducing more sidebranches of different resonance frequencies on one side of a duct section is investigated. The corresponding sidebranch interactions are also examined. It is hoped that this study can reveal the optimum low frequency performances one can expect of sidebranch arrays. The sound attenuation magnitudes, the working bandwidths and the continuity of the TL spectra are chosen to be the performance indicators.

2. Array configurations

Fig. 1 illustrates the schematics of an array of 11 sidebranches installed flushed with one of the walls of a rectangular duct having a cross-section dimension of a by b ($b > a$) and the nomenclatures of this study. The ratio b/a is set equal to π/e (where e is the natural number) in order to avoid the degenerated duct modes. There are two ways to introduce more sidebranches without increasing the overall array length. The first one is to reduce the sidebranch width w to accommodate more sidebranches in the longitudinal direction. However, w ($= 0.1a$) is already small and it is found from a preliminary study with air damping ignored that too small a sidebranch width w will result in very spurious TL spectra with undesirably low TL troughs between the TL peaks. In the presence of air damping, the magnitude of the mouth impedance is expected to increase as w

decreases such that the sidebranches will be acoustically harder, resulting in poor sound attenuation performance. The second approach is to reduce the sidebranch span s such that more sidebranch arrays of the same overall length can be added side-by-side with each other. Again, s cannot be too small, but there is room for its reduction. This approach is adopted in the present study. The thicknesses of the walls separating two coupling arrays and that separating two adjacent sidebranches are both fixed at $0.1w$.

For simplicity, the linear sidebranch length variation model of Tang [12] is adopted in the present study. The length of the i th sidebranch in the array, l_i , is

$$l_i = l_{max} - \frac{i-1}{n-1}(l_{max} - l_{min}), \quad (1)$$

where $n = 11$, while l_{max} and l_{min} are the lengths of the longest and shortest sidebranches. Fig. 2 shows the effect of s on the TL across a single sidebranch array with l_{max} and l_{min} equal $1.025a$ and $0.525a$ respectively in the undamped condition. The numerical method adopted is described in Section III. As s is reduced, the TL spectra become more spurious with more discrete sharp TL peaks. The benefit of bandwidth widening by sidebranch interactions is gradually lost. The magnitudes of the TL peaks become stronger while those of the troughs go lower as s decreases. The TL peak frequencies are also closer to the fundamental quarter-wavelength tube resonance frequencies when s is small. Though a smaller s would mean the possibility of incorporating more sidebranch arrays of different length series in the silencing assembly, this will also increase the complexity of the device. It is believed that $s = 0.5b$ is a legitimate choice.

The two sidebranch arrays in this study are hereinafter referred as Arrays A and B. The lengths of the sidebranches in Array A follow those presented in Eq. (1) :

$$l_{i,A} = a - 0.05a(i-1) \quad (2a)$$

while those in Array B are

$$l_{i,B} = 1.025a - 0.05a(i-1) \quad (2b)$$

where the suffices A and B denote quantities related to Arrays A and B respectively in the rest of this paper. Though the lengths of the sidebranches in the two arrays are similar, the TL peak frequencies associated with Array B are close to those of the TL troughs of Array A and vice versa. A more broadband performance of the coupled arrays is thus anticipated.

The results of Tang [12] indicate that the TL across the focussed duct section can be increased by coupling an identical array on the opposite side of the duct. There are two arrays and thus there are several possible configurations of coupled array assembly. Fig. 3 summarizes the basic test cases in this study. The suffix ‘rev’ represents the cases where the position order of the sidebranch tubes in the lower array is reversed. There are also cases where the separating walls between the two side-by-side arrays are removed. A suffix ‘-w’ will be added to the corresponding case codes. The present study is mainly focussed at frequencies below that of the first asymmetric eigen-mode of the duct, that is, $kb < \pi$ or $ka < 0.86\pi$. A design formed by one Array A and one Array B is hereinafter referred to as a coupled array. The Array A and Array B with $s = 0.5b$ are called sub-arrays in the foregoing discussions. They are the basic elements that make up the other coupled array designs.

3. Numerical method

The finite-element solver implemented in COMSOL [13] is used in the present study to solve, in the frequency domain, the wave equation:

$$\nabla^2 p + k^2 p = 0, \quad (3)$$

where p is the sound pressure and k the wavenumber. The longitudinal span of the main computational domain is set to be $-5a \leq x \leq 6a$. The plane $x/a = 0$ represents the entrance of the sidebranch array section. A unit longitudinal plane wave is injected into this domain at $x = -5a$. The boundary condition at this inlet position is set according to the second order boundary radiation condition of Givoli and Neta [14]. Under the present setting, this boundary condition is actually the same as that adopted in the previous studies of the authors (for instance, Tang [12]). A perfectly

matched layer [15] is specified at $x > 6a$. The corresponding scaling factor and curvature parameter are both set equal to unity. The ‘polynomial’ coordinate stretching is adopted. The length of this layer is one-third that of the main computational domain in order to ensure that there is no significant reflection at the end of the main computational domain. As all higher duct modes can only exist in form of evanescent waves in the present frequency range of interest, they should have largely decayed, and thus are insignificant, at the two extreme ends of the main computational domain. All other surfaces are set acoustically hard.

Air is the medium for sound propagation in the present study. As in Nelson et al. [16] and Lau and Tang [17], the computational domain is set slightly absorptive to sound. An attenuation coefficient of 0.02 Np/m is adopted in this study regardless of the sound frequency. This very small absorption helps numerical convergence and avoids unrealistically small meshes, especially at high frequencies. It only results in an approximately 0.16 dB transmission loss when the sidebranch array section is replaced by a straight duct section over the whole frequency range of interest. This loss is insignificant when compared to those resulted from the arrays presented in Section IV. Without this absorption, the present setting reproduces the results of Tang [12] at frequencies before the cut-on of the first higher spanwise duct mode.

Unstructured tetrahedral and triangular meshes are adopted in this study [18]. There are also triangular meshes on surfaces, edge elements along edges and vertex elements at corners. The maximum mesh size is kept less than 1/6 of the shortest wavelength included. For the tetrahedral meshes, the curvature factor is fixed at 0.2 for all the meshes, while the average growth rate and the average mesh quality index are 1.74 and 0.73 respectively. The variations of the latter two indices across meshes are very small. For the triangular meshes, the average mesh quality index is approximately 0.92. Table 1 summarizes the information of the numerical meshes adopted in this study. Though the minimum mesh quality indices are small, the number of meshes having such a small quality index is in fact very limited. Fig. 4 illustrates the quality index distributions of the $[A \oplus B]_{-w}/[A \oplus B]_{-w,rev}$ mesh with a bin-width of 0.01. One can observe that over 90% of the

tetrahedral meshes are with a mesh quality index higher than 0.5. The probability distributions are very much negatively skewed. The quality index distributions for all the other meshes used in this study are very similar to those shown in Fig. 4 and thus they are not presented. A further reduction of the mesh size does not result in any meaningful changes in the numerical results.

4. Results and discussions

4.1. Standalone Coupled Array

As the effective frequency range of Arrays A and B is $0.4 < ka/\pi < 0.8$ (Fig. 2), the foregoing discussions will be focused in this frequency range. Fig. 5 illustrates the frequency variations of the TL s of $[A \oplus B]$ and $[A \oplus B]_{-w}$. Those of $[A]$ and $[B]$ are also presented for the sake of easy comparison. Though the results in Fig. 2 suggest that the acoustical performance of the array is reduced when its span s decreases, the side-by-side arrangement of $[A]$ and $[B]$ of $s = 0.5b$ does not cause the kind of performance deterioration shown in Fig. 2. In fact, the characteristics of the frequency variation of TL of $[A \oplus B]_{-w}$ are very similar to those of $[A]$ or $[B]$. The sound transmission loss mechanisms are very similar to those of $[A]$ or $[B]$ which have been discussed in Tang [14]. Thus, they are not discussed here. However, one should note that the overall performance of $[A \oplus B]_{-w}$ is slightly better than those of $[A]$ and $[B]$ on average. $[A \oplus B]$ gives more TL peaks than $[A]$, $[B]$ and $[A \oplus B]_{-w}$ within the frequency range of interest. There is also higher chance that $[A \oplus B]$ can provide satisfactory noise reduction than the other three designs.

A strong peak is observed at $ka/\pi \sim 0.4644$. This frequency is very close to that of the first TL peak of $[A]$ and that of the second TL peak of $[B]$. Fig. 6a illustrates the iso-surfaces of the sound pressure (real part) within the duct section installed with $[A \oplus B]$ at $ka/\pi = 0.4644$. The concerted resonance at the entrance of the $[A]$ and $[B]$ sub-arrays results in such a strong transmission loss of $[A \oplus B]$. The TL peaks of $[A \oplus B]$ for $ka/\pi > 0.48$ are mainly due to the concerted strong pressure fluctuations in the two sub-arrays or the coupled resonance between

adjacent tubes in one of the sub-arrays. The latter is more pronounced at higher frequencies. Some examples of these phenomena are given in Figs. 6b and 6c.

$[A \oplus B]$ has a problem at $ka/\pi = 0.4426$ where an abrupt and sharp TL dip is observed. The wall between the two sub-arrays that make up $[A \oplus B]$ gives rise to a discontinuity midway along the duct span. The acoustical behaviours inside the sidebranches of the two arrays can thus be different under the same excitation. One can observe from Fig. 6d that the strong longitudinal pressure fluctuations inside the first two sidebranches of the two sub-arrays are out-of-phase. This results in a dipole radiation and thus a weak cancelling wave downstream inside the main duct downstream. The corresponding TL is therefore weak. The TL troughs found at higher frequencies are due to the actions of three/four nearby sidebranches in general. This interaction gives out dipole radiation along the length and span of the duct, which is somewhat like an asymmetric quadrupole radiation. Typical examples of such sidebranch coupling are given in Figs. 6e and 6f.

4.2. Coupled Arrays on Opposite Duct Walls

For the cases of two coupled arrays installed on opposite duct walls, there are four ways the sidebranch array coupling can be done as shown in Fig. 3. Fig. 7 illustrates the TL s of $[A \oplus B]/[A \oplus B]$ and $[A \oplus B]/[B \oplus A]$ with and without the middle sidebranch walls. The data of the full span $[A]/[A]$ and $[B]/[B]$ are also presented for the sake of easy comparison. In general, the coupling of sidebranch arrays on opposite duct walls increases the TL s at frequencies below the first spanwise eigenmode frequency of the duct ($kb = \pi$). The performances of $[A \oplus B]/[A \oplus B]$ and $[A \oplus B]/[B \oplus A]$ for $kb < \pi$ are very similar, except that there is a very small shift in the frequencies of TL peaks.

The performances of $[A \oplus B]/[A \oplus B]$ and its derivatives, especially that of $[A \oplus B]_{-w}/[A \oplus B]_{-w}$, at $kb \sim \pi$ are in general worse than those of the $[A \oplus B]/[B \oplus A]$ family. It is because of the stronger forcing of the first spanwise higher acoustic mode by the $[A \oplus B]/[A \oplus B]$ family (not shown here). The $[A \oplus B]$ and $[B \oplus A]$ tend to excite this higher spanwise mode in an out-of-phase manner and thus the much weaker spanwise mode excitation of the $[A \oplus B]/[B \oplus A]$ family. The higher acoustic

modes are left to further investigations. Unless otherwise stated, the foregoing analysis will be focused on the $[A \oplus B]/[B \oplus A]$ family.

The overall performances in term of sound power transmission loss of the three setups of the $[A \oplus B]/[B \oplus A]$ family are very similar. As expected $[A \oplus B]/[B \oplus A]$ and $[A \oplus B]/[B \oplus A]_{-w}$ give more TL peaks. The former results in sharp and strong TL peaks, but it also gives rise to deeper TL toughs. The TL of the latter can be maintained at relatively high level within the frequency range of interest. The designs $[A \oplus B]_{-w}/[B \oplus A]_{-w}$ and $[A \oplus B]/[B \oplus A]$ are less preferable as there are many occasions that they result in TL toughs lower than those of $[A \oplus B]/[B \oplus A]_{-w}$. The performance of $[A \oplus B]_{-w}/[B \oplus A]_{-w}$ is similar to those of $[A]/[A]$ and $[B]/[B]$. The introduction of sub-arrays has improved the acoustical performance of the sidebranch array in terms of sound power transmission uniformity and the magnitude of the sound transmission loss across the frequency range of interest.

The strong TL dip of $[A \oplus B]$ at $ka/\pi = 0.4426$ (Fig. 5) is again observed in these coupled cases but at a different frequency. Fig. 8a shows the sound pressure iso-surfaces of $[A \oplus B]/[B \oplus A]$ at similar dip frequency. A quadrupole-like radiation is resulted because of the out-of-phase resonances of the $[A]$ and $[B]$ sub-arrays. Since quadrupole radiation is weak, the cancelling plane wave so generated should be weak and thus the appearance of this TL dip. The TL peak at $ka/\pi = 0.4452$ preceding this dip is due to the cancelling wave resulted from the relatively in-phase monopole radiations from the $[A]$ sub-arrays as shown in Fig. 8b. The sound pressures inside the other branches are very weak.

Fig. 8c illustrates the sound pressure iso-surfaces of $[A \oplus B]/[B \oplus A]_{-w}$ at the corresponding dip frequency. For this asymmetric $[A \oplus B]/[B \oplus A]_{-w}$ design, the frequency responses of the upper and lower arrays are very different. At the dip frequency, there is no resonance in the lower array and the sound pressure within its first sidebranch is relatively uniform. The wave interactions in the upper array are very similar to that of $[A \oplus B]$ (c.f. Fig. 5a). However, the action of the velocity oscillation at the mouths of the first several sidebranches of the lower array can still produce a

cancelling wave downstream even the dipole-like radiation of the upper array fails to do so. The relatively uniform sound pressure inside the lower array at low frequency tends to smooth out the irregularity observed in the $[A\oplus B]/[B\oplus A]$ case discussed in the previous paragraph. This is also the main reason why the TL s of $[A\oplus B]/[B\oplus A]_{-w}$ can be maintained at relatively higher level than the other two designs in general. This will be discussed further later.

The TL peaks are also resulted from the concerted resonances inside the sidebranches of the tow coupled arrays. For the $[A\oplus B]/[B\oplus A]$ design, the peaks are similar in magnitudes in general. The relatively higher peaks are due to the strong acoustical activities within two consecutive sidebranches of the $[A]$ sub-arrays as shown in Fig. 9a. In order to better illustrate the sound fields inside the sidebranches, the sound pressure iso-surfaces viewed from the two opposite sides of the main duct are presented in each sub-Fig. of Fig. 9. Under this condition, the resonance takes place inside the third and the fourth sidebranches of the $[A]$ sub-array, while the in-phase interaction takes place in the sidebranches of the $[A]$ sub-array at the opposite corner of the duct cross-section. The acoustical activities in the $[B]$ sub-arrays are insignificant. The relatively lower peaks are the results of the interaction between nearby sidebranches of the $[A]$ and $[B]$ sub-arrays as shown in Fig. 9b. The interaction results in quadruple-like cancelling field as discussed before in Fig. 8a. The cancelling wave is expected to be weaker than that shown in Fig. 9a, and thus a relatively lower TL . In this case, the main resonance takes place within one sidebranch of the $[B]$ sub-array. It is found that the TL troughs between the abovementioned TL peaks are associated with a situation where there are strong acoustical activities in three consecutive sidebranches of either the $[A]$ or the $[B]$ sub-arrays. Typical examples are shown in Figs. 9c and 9d.

For the $[A\oplus B]/[B\oplus A]_{-w}$ design, the magnitudes of adjacent TL peaks are very different. However, the wave interactions which are associated with the alternatively higher and lower TL peaks are similar to those observed in the $[A\oplus B]/[B\oplus A]$ case as shown in Fig. 10. One major difference is that the sound pressure spanwise variation within the lower $[B\oplus A]_{-w}$ array is very small. This relatively uniform sound pressure helps maintaining the TL at relatively higher level

than those in the other designs of the family. The wave interactions for the $[A\oplus B]/[A\oplus B]$ cases with and without partition walls are very similar to those of their $[A\oplus B]/[B\oplus A]$ counterparts for $ka/\pi < 1$ and thus are not presented.

4.3. Coupled Arrays with Opposite Sidebranch Sequence

The arrangement sequence of the sidebranches in the two arrays has significant impacts on the TL . Fig. 11a illustrates the TL s of the coupled arrays in previous section but with the sidebranch arrangement sequences of the lower arrays reversed (that is, $[A\oplus B]/[B\oplus A]_{\text{rev}}$ and its derivatives). First of all, the asymmetric sidebranch arrangement tends to excite the first odd acoustic mode across the duct width. The performances of the coupled arrays are thus poor as ka/π approaching unity. The corresponding results of the $[A\oplus B]/[A\oplus B]_{\text{rev}}$ family, except those of $[A\oplus B]/[A\oplus B]_{\text{rev}}$, are nearly the same as those of their counterparts in the $[A\oplus B]/[B\oplus A]_{\text{rev}}$ family (Fig. 11b).

The reversed sidebranch sequence lowers significantly the low frequency performances of all the coupled arrays, except at around $ka/\pi \sim 0.42$, where the strong TL peaks are independent of sidebranch resonance characteristics. The corresponding sound fields in $[A\oplus B]/[B\oplus A]_{\text{rev}}$ at $ka/\pi = 0.4128$ viewed from the two opposite sides of the main duct are illustrated in Fig. 12a. The abrupt and large change in acoustic impedance at the two ends of this duct section gives rise to strong sound pressure fluctuations inside the longest sidebranches of each sub-array. The vigorous air movements at their mouths create strong forward and backward travelling waves. The length of the 11-tube sidebranch array, L_{11} , is $1.2a$ and the first frequency of high sound transmission loss as estimated using the expansion chamber TL formula is $kL_{11}/\pi = 0.5 \Rightarrow ka/\pi = 5/12 \approx 0.4167$. This strong TL peak is thus due to some sort of longitudinal resonance across the length of the coupled array duct section in a way similar to that inside a regular expansion chamber. The TL dip at around $ka/\pi \sim 0.46$ is due to acoustic resonance along the longest sidebranches (not shown here). One can also observe the small TL peak and dip in between the strong TL peak and dip. The corresponding mechanisms have been discussed before and thus are not repeated here.

For the designs $[A \oplus B]/[B \oplus A]_{\text{rev}}$ and $[A \oplus B]/[A \oplus B]_{\text{rev}}$ for $ka/\pi > 0.54$, the TL troughs are in general associated with strong acoustical pressure inside one sidebranch of one sub-array together with strong out-of-phase pressures inside two adjacent consecutive sidebranches of the other array. An example is illustrated in Fig. 12b. The TL peaks are found when much stronger sound pressure is excited in one of the sub-arrays than in the others (for instance, Fig. 12c). One can observe that the sound pressures within the upper array, whose longest sidebranches are facing the incident sound, are relatively weak throughout the process. This is probably due to the smaller reflection at the leading edge of the lower array resulted from the smaller wall impedance change there than that occurs at the leading edge of the upper array. The sound pressure fluctuations near to the lower array are stronger and thus the stronger excitation to its sidebranches.

For $0.42 < ka/\pi < 0.54$, the abovementioned expansion chamber effect and the low resonance frequencies of the longer sidebranches of the $[A]$ and $[B]$ sub-arrays tend to maintain strong pressure fluctuations inside the first several sidebranches of the upper array (not shown here). However, unlike the un-reversed cases, the strong acoustical activities of the upper and lower arrays are more often out-of-phase and not occur on the same axial plan (c.f. Fig. 8a and Fig. 12d). It is conjectured that the expansion chamber effect has limited the TL across the duct section installed with the sidebranch arrays. These out-of-phase pressure fluctuations, which take place within three to four sidebranches of each sub-array, tend to reduce the magnitude of the cancelling wave and further lower down the TL . Such kind of cancelling pressure fluctuations is not found in the coupled arrays with at least one side wall between the $[A]$ and $[B]$ sub-array removed. The low frequency performances of $[A \oplus B]/[B \oplus A]_{\text{rev}}$ (and also $[A \oplus B]/[A \oplus B]_{\text{rev}}$) is thus the worst in this design family.

It should be noted that the coupled arrays with reversed sidebranch arrangement sequence is not preferable compared to their un-reversed counterparts as they can only offer better TL within a relatively narrow bandwidth.

5. Conclusions

The wave interactions that result in the sound transmission losses across coupled sidebranch arrays in an infinitely long rectangular duct are investigated numerically using the finite-element-method in this study. Two sidebranch arrays with different branch length series and with no overlapping of resonance frequencies are considered in this study. Each sidebranch array consists of eleven narrow sidebranches and its width is half the spanwise width of the duct. The present study is focussed at frequencies below the first higher duct mode cut-off frequency. The spanwise width of the duct is longer than its vertical width.

For the case of a side-by-side coupled array on one single duct wall, the sound transmission loss peaks come basically from either the concerted strong pressure fluctuations in the two coupled arrays or the resonance between adjacent sidebranches in one of these arrays. The latter is more pronounced at higher frequencies. The sound transmission loss troughs are usually the result of the joint action of three to four adjacent sidebranches, forming some sort of asymmetric quadrupole cancelling wave fields. The performance of the coupled array is somewhat similar to those of the individual arrays making up the coupled array if the separating walls between the arrays are removed.

For the cases with two coupled arrays mounted on opposite duct walls and with the longest sidebranch of each sub-array facing the incoming incident planar sound wave, the spectral variations of the sound transmission losses across the coupled arrays are basically not affected much by the locations of the sub-arrays before the cut-on of the first higher duct mode. Stronger and more uniform sound transmission losses across the frequency range of interest than the single coupled array are observed. The combined in-phase action of the two coupled arrays results in stronger sound cancelling capacity. However, the asymmetric quadrupole sound field is generated when the velocity oscillations in the two coupled arrays are out-of-phase, resulting in relatively lower sound transmission loss. The performance of this array system can be improved by removing the sub-array separating wall of one of the coupled arrays as the abovementioned out-of-phase

velocity oscillations is less likely to occur because of the then very different frequency characteristics of the two coupled arrays.

The low frequency performance of the two coupled arrays is significantly reduced when the sidebranch arrangement sequence of one of the coupled arrays is reversed. It appears that the array section behaves like an expansion chamber at low frequencies. The array systems with the sub-array separating walls intact are the worst designs. The out-of-phase oscillations inside the two coupled arrays, which take place at different axial positions within the array section, tend to weaken further the corresponding sound transmission losses. At higher frequencies, the coupled array with its longest sidebranch facing the incoming sound is much less responsive acoustically than the other array.

Acknowledgements

The financial support of the Research Grants Council, The Hong Kong Special Administration Region Government is gratefully acknowledged (Project No. PolyU5250/13E).

References

- [1] Harris M. Handbook of Noise Control. New York: McGraw-Hill; 1979.
- [2] Huang L, Choy YS. Vibro-acoustics of three dimensional drum silencer. J Acoust Soc Am 2005;118(4):2313–2320.
- [3] Tang SK. Vortex sound in the presence of a low Mach number flow across a drum-like silencer. J Acoust Soc Am 2011;129(5):2830–2840.
- [4] Allam S, Åbom M. A new type of muffler based on microperforated tubes. ASME Trans J Vib Acoust 2011;133(3):031005.
- [5] Canevet G. Active sound absorption in an air conditioning duct. J Sound Vib 1978;58(3):333–345.
- [6] Wells RJ. Acoustical plenum chambers. Noise Control 1958;4:9–15.

- [7] Tang SK. On sound transmission loss across a Helmholtz resonator in a low Mach number flow duct. *J Acoust Soc Am* 2010;127(6):3519–3525.
- [8] Salemat, Dickey NS, Novak JM. The Herschel-Quincke tube: A theoretical, computational and experimental investigation. *J Acoust Soc Am* 1994;96(5):3177–2185.
- [9] Howard Q, Craig RA. Noise reduction using a quarter wave tube with different orifice geometries. *Appl Acoust* 2014;76:180–186.
- [10] Seo SH, Kim YH. Silencer design by using array resonators for low frequency band noise reduction. *J Acoust Soc Am* 2005;118(4):2332–2338.
- [11] Howard Q, Cazzolato BS, Hansen CH. Exhaust stack silencer design using finite element analysis. *Noise Control Eng J* 2000;48(4):113–120.
- [12] Tang SK. Narrow sidebranch arrays for low frequency duct noise control. *J Acoust Soc Am* 2012;132(5):3086–3097.
- [13] COMSOL, Acoustics Module User’s Guide, version 5.1, 2015.
- [14] Givoli, Neta B. High-order non-reflecting boundary scheme for time-dependent waves. *J Comput Phys* 2004;186(1):24–46.
- [15] Jin JM. *Theory and Computation of Electromagnetic Waves*. New Jersey: Wiley; 2010.
- [16] Nelson PA, Curtis ARD, Elliott SJ, Bullmore AJ. The active minimization of harmonic enclosed sound field, Part I: theory. *J Sound Vib* 1987;117(1):1–13.
- [17] Lau SK, Tang SK. Sound fields in a slightly damped rectangular enclosure under active control. *J Sound Vib* 2000;238(4):637–660.
- [18] COMSOL, COMSOL Multiphysics Reference Guide, version 5.1, 2015.

Captions

- Figure 1 Schematics of the basic sidebranch array setup and nomenclatures.
- Figure 2 Effects of sidebranch spanwise width on sound transmission loss across Array B.
 — : $s = b$; - - - : $s = 0.6b$; — · — : $s = 0.2b$; — · · — : Array A, $s = b$.
- Figure 3 Sidebranch array configurations adopted in this study.
- Figure 4 Quality index distributions of the $[A \oplus B]_{-w}/[A \oplus B]_{-w,rev}$ mesh.
 Tetrahedral mesh : — : cumulative; — · — : probability distribution;
 Triangular mesh : - - - - : cumulative; — · · — : probability distribution.
- Figure 5 Sound transmission loss across $[A \oplus B]$ and $[A \oplus B]_{-w}$.
 — : $[A \oplus B]$; - - - - : $[A \oplus B]_{-w}$; — · — : $[B]$, $s = b$; — · · — : $[A]$, $s = b$.
- Figure 6 Iso-surfaces of sound pressures inside $[A \oplus B]$ at some TL peak and trough frequencies.
 Peaks : (a) $ka/\pi = 0.4644$; (b) $ka/\pi = 0.5230$; (c) $ka/\pi = 0.6017$.
 Troughs : (d) $ka/\pi = 0.4487$; (e) $ka/\pi = 0.5309$; (f) $ka/\pi = 0.5746$.
- Figure 7 Sound transmission loss across coupled sidebranch arrays.
 (a) $[A \oplus B]/[A \oplus B]$ family; (b) $[A \oplus B]/[B \oplus A]$ family.
 — : $[A \oplus B]_{-w}/[A \oplus B]_{-w}$ in (a) and $[A \oplus B]_{-w}/[B \oplus A]_{-w}$ in (b);
 - - - - : $[A \oplus B]/[A \oplus B]_{-w}$ in (a) and $[A \oplus B]/[B \oplus A]_{-w}$ in (b);
 — — : $[A \oplus B]/[A \oplus B]$ in (a) and $[A \oplus B]/[B \oplus A]$ in (b);
 — · — : $[A]/[A]$, $s = b$; — · · — : $[B]/[B]$, $s = b$.
- Figure 8 Sound pressure iso-surfaces in $[A \oplus B]/[B \oplus A]$ and $[A \oplus B]/[B \oplus A]_{-w}$ near the first relatively prominent TL dips.
 (a) $[A \oplus B]/[B \oplus A]$, $ka/\pi = 0.4478$; (b) $[A \oplus B]/[B \oplus A]$, $ka/\pi = 0.4452$;
 (c) $[A \oplus B]/[B \oplus A]_{-w}$, $ka/\pi = 0.4434$.

Figure 9 Typical sound pressure iso-surfaces in $[A \oplus B]/[B \oplus A]$ at frequencies of TL peaks for $kb/\pi < 1$ and $ka/\pi > 0.5$.

(a) $ka/\pi = 0.5466$; (b) $ka/\pi = 0.5055$; (c) $ka/\pi = 0.5265$; (d) $ka/\pi = 0.5405$.

Figure 10 Sound pressure iso-surfaces in $[A \oplus B]/[B \oplus A]_{-w}$ at some TL peak frequencies.

(a) $ka/\pi = 0.5633$; (b) $ka/\pi = 0.5685$; (c) $ka/\pi = 0.5764$.

Figure 11 Sound transmission loss across coupled arrays with reversed sidebranch arrangement sequence.

(a) $[A \oplus B]/[B \oplus A]_{\text{rev}}, [A \oplus B]/[B \oplus A]_{-w, \text{rev}}$ and $[A \oplus B]_{-w}/[B \oplus A]_{-w, \text{rev}}$;

(b) $[A \oplus B]/[A \oplus B]_{\text{rev}}, [A \oplus B]/[A \oplus B]_{-w, \text{rev}}$ and $[A \oplus B]_{-w}/[A \oplus B]_{-w, \text{rev}}$.

———— : $[A \oplus B]_{-w}/[B \oplus A]_{-w, \text{rev}}$ in (a) and $[A \oplus B]_{-w}/[A \oplus B]_{-w, \text{rev}}$ in (b);

— — — — : $[A \oplus B]/[B \oplus A]_{-w, \text{rev}}$ in (a) and $[A \oplus B]/[A \oplus B]_{-w, \text{rev}}$ in (b);

— — : $[A \oplus B]/[B \oplus A]_{\text{rev}}$ in (a) and $[A \oplus B]/[A \oplus B]_{\text{rev}}$ in (b);

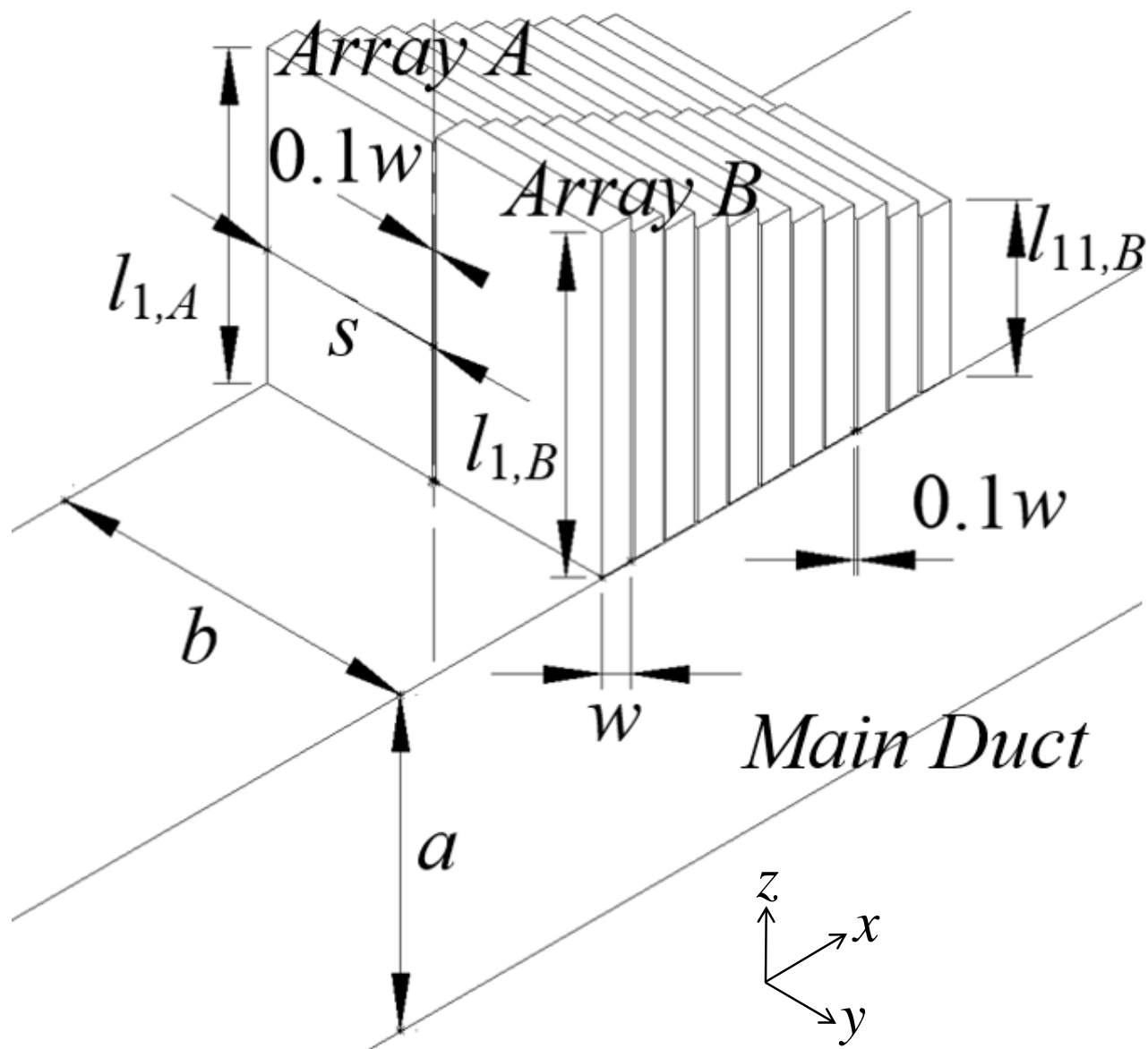
— · — : $[A]/[A]_{\text{rev}}, s = b$; — · · — : $[B]/[B]_{\text{rev}}, s = b$.

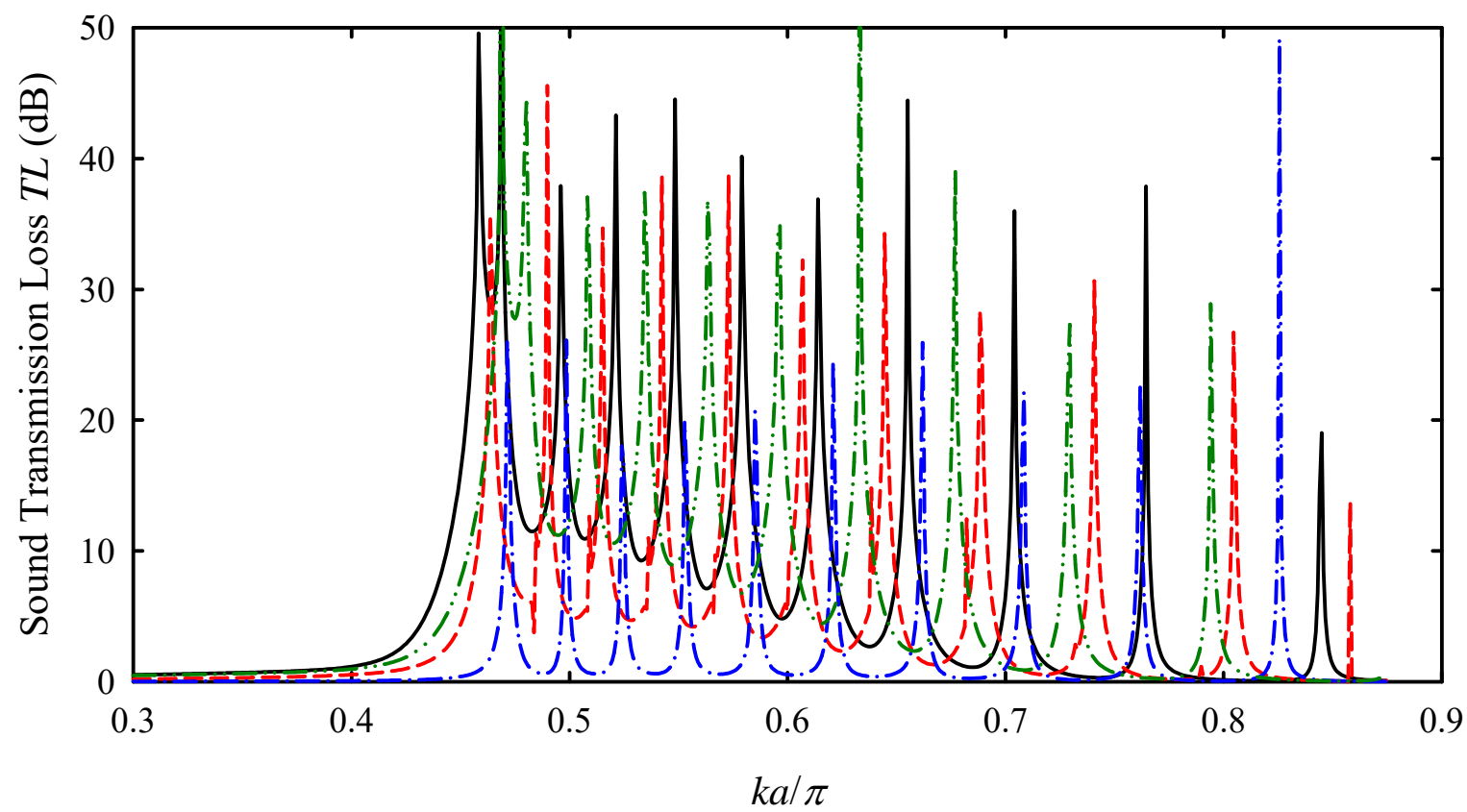
Figure 12 Examples of sound pressure iso-surfaces within $[A \oplus B]/[B \oplus A]_{\text{rev}}$.

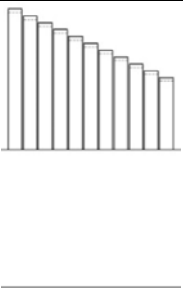
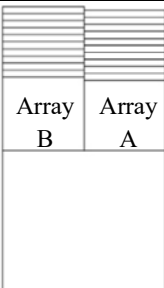
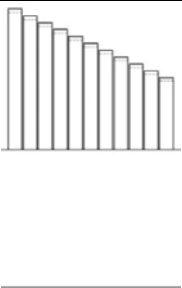

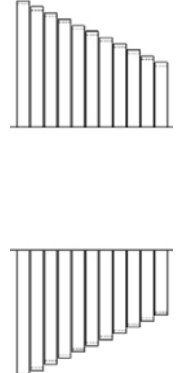
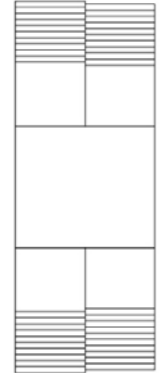
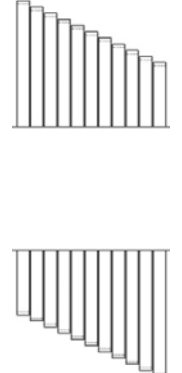
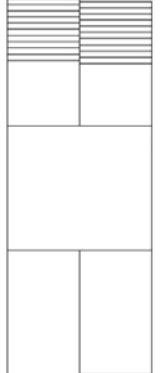
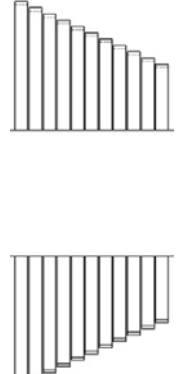
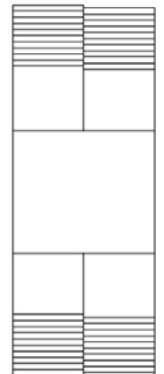
(a) $ka/\pi = 0.4128$; (b) $ka/\pi = 0.5746$; (c) $ka/\pi = 0.5808$; (d) $ka/\pi = 0.5134$.

Table 1
Details of the meshes adopted in the present study

Mesh Type	Mesh Data	Array Design					
		[A], [B]	[A⊕B], [A⊕B] _{-w}	[A]/[A], [A]/[A] _{rev} , [B]/[B], [B]/[B] _{rev}	[A⊕B]/[A⊕B], [A⊕B]/[B⊕A], [A⊕B]/[A⊕B] _{rev} , [A⊕B]/[B⊕A] _{rev}	[A⊕B]/[A⊕B] _{-w} , [A⊕B]/[B⊕A] _{-w} , [A⊕B]/[A⊕B] _{rev,-w} , [A⊕B]/[B⊕A] _{rev,-w}	[A⊕B] _{-w} /[A⊕B] _{-w} , [A⊕B] _{-w} /[B⊕A] _{-w} , [A⊕B] _{-w} /[A⊕B] _{rev,-w} , [A⊕B] _{-w} /[B⊕A] _{rev,-w}
Tetrahedral	Number of elements	312344 – 312519	321334 – 324600	612624 – 625116	633296 – 636639	636663 – 637621	636299 – 638714
	Minimum element quality	0.0715 – 0.0987	0.0788 – 0.0825	0.0641 – 0.0968	0.0714 – 0.1042	0.1111 – 0.1138	0.0881 – 0.1081
	Average element quality	0.7268 – 0.7277	0.7272 – 0.7275	0.7265 – 0.7299	0.7282 – 0.7285	0.7277 – 0.7282	0.7264 – 0.7268
	Maximum growth rate	3.762 – 3.908	3.661 – 4.093	3.883 – 4.970	3.858 – 4.393	3.848 – 4.174	3.925 – 4.220
	Average growth rate	1.742 – 1.745	1.741 – 1.746	1.739 – 1.744	1.738 – 1.741	1.740 – 1.743	1.744 – 1.745
Triangular	Number of elements	44550 – 44590	46724 – 47458	74692 – 87122	90740 – 91236	91693 – 91819	92780 – 92900
	Minimum element quality	0.2671 – 0.2744	0.2640 – 0.2724	0.2610 – 0.2744	0.4068 – 0.4127	0.2724 – 0.2726	0.2724
	Average element quality	0.9206 – 0.9216	0.9197 – 0.9228	0.9158 – 0.9234	0.9233 – 0.9235	0.9228 – 0.9231	0.9212 – 0.9220
Edge	Number of elements	3377 – 3387	4065 – 4151	6313 – 6513	8091 – 8114	7981 – 7982	7868 – 7870
Vertex	Number of elements	100	166 – 188	188	364	342	320





Case Code	Configuration		Case Code	Configuration	
$[A \oplus B]$			$[A] \text{ or } [B]$		
$[A \oplus B]/[A \oplus B]$			$[A \oplus B]/[A \oplus B]_{\text{rev}}$		
$[A \oplus B]/[B \oplus A]$			$[A \oplus B]/[B \oplus A]_{\text{rev}}$	